### MSEC2024-124600

### PARTICLE ANALYSIS FROM HETEROGENEOUS BACKGROUND WITH DEEP LEARNING TOOL

Adeeb Ibne Alam
Mechanical Engineering Department
University of Maine, Orono
Maine, ME

Md Rafiul Hassan, Ph.D.
Computer Science Department
University of Maine at Presque Isle,
Maine. ME

Bashir Khoda, Ph.D.

Mechanical Engineering Department
University of Maine, Orono
Maine. ME

### **ABSTRACT**

The performance of conventional image processing techniques is highly dependent on many parameters like image quality, light source, background surface texture, optimal threshold value and particle morphology. However, during intermediate stages of manufacturing processes (such as continuous deposition, coating, mixing, and transfer), complex backgrounds can arise from heterogeneous particle-substrate (HPS) systems. In such HPS environments, particles become integrated with substrates or suspended in liquid carriers or etching media, making them challenging to identify using traditional particle analysis tools and techniques. In response to this challenge, a deep learning object detection algorithm (YOLO) has been put into practical use. Initially, an HPS (heterogeneous particle-substrate) system was created using a wet-deposition particle transfer process that involved the immersion of poly-disperse particles on to a cylindrical substrate. By manipulating the capillary number in the wetdeposition process, four distinct HPS morphologies were captured, each characterized by variations in image heterogeneity. These morphologies were subsequently subjected to detailed analysis with neural network-based AI algorithm. The proposed artificial intelligence tool has demonstrated an impressive ability to identify and analyze poly-dispersed particles within HPS morphologies, achieving an accuracy rate of over 97%. We can evaluate the quality of sorting by calculating the particle size distribution using the proposed method and find the ideal process parameters for the particle transfer process. The results of this study, outlined in this paper. underscore the potential of deep learning as a particle analysis tool for in-situ applications, even in environments with heterogeneous backgrounds. This developed tool holds promise for various manufacturing processes, including semiconductor industries, high-density powder-based 3D printing, powder metallurgy, refractory coatings in harsh environments, and particle sorting, among others.

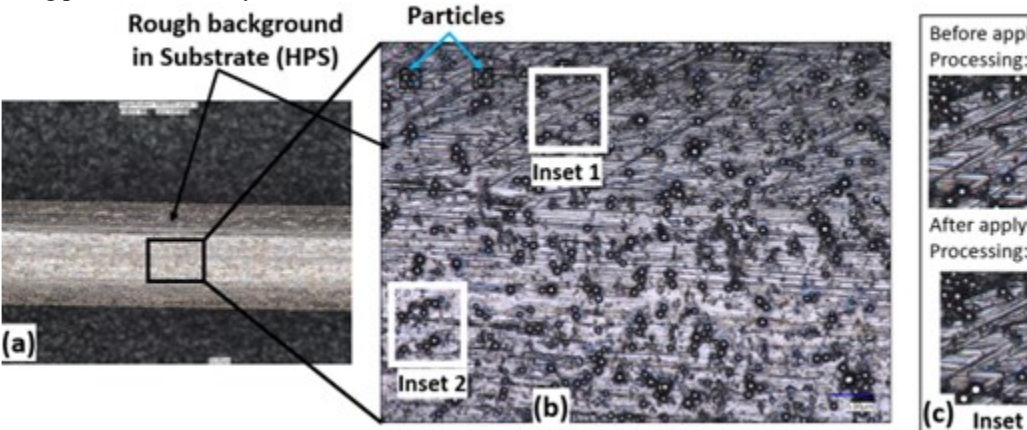
# Keywords: Heterogeneous image, Particle metrology, Image Processing, YOLO.

### 1. INTRODUCTION

Powder particles or granular materials are important forms of material which are direct or indirect input in manufacturing processes including semiconductor manufacturing, additive manufacturing [1] and powder metallurgy [2]), transforming surface (i.e., rust protection [3-5], controlling roughness and conductivity [6], meta surface [7, 8], self-cleaning hydrophilic [9] [10]), enhancing properties (i.e., viscosity modifier [11]). As a result, their size and distribution analysis has become a crucial aspects of metrology research. The image analysis tools drive researchers to extract information from the microscopic and spectroscopic images of virgin powder. These tools are often user specific that involve semantic knowledge and produce qualitative results. A widely used, conventional image processing tool, applied for general purpose is ImageJ developed by National Institute of Health (NIH) [12]. Kumara et al. performed image analysis of gravels (2-19 mm) through ImageJ software [13]. They captured the 2D images of gravels in a transparent sheet as background using digital single-lens reflex (DSLR) camera. Berardi et al. studied the size expansion of tablets during disintegration for pharmaceutical applications [14]. They also captured images of tablets with DSLR camera and performed image analysis through ImageJ to determine projected area and aspect ratio. Lee et al. [15] analyzed the confocal laser scanning microscopy (CLSM) images of pellet coating using ImageJ and calculated the coating thickness from the irregular shape measurement of pellets. He et al. [16] studied the influence of process parameters including solution concentration, collection distance, voltage and collection speed on the diameter and orientation of nanofibers made of electrospinning process. They investigated the surface morphology of nanofibers using SEM images and analyzing it through ImageJ. Depending upon the sample and imaging conditions, this software sometimes omit particles and incorrectly identify particle boundaries which requires labor intensive post-processing.

Apart from the ImageJ software, some automatic and semiautomatic software packages were also used to determine particle size distribution. Mondini et al. [17] developed a custom software named Pebbles to measure the surface morphology and diameter of nanoparticles. Phromsuwan et al. [18] analyzed the nanoparticles size distribution in transmission electron microscopy (TEM) images using an automated image processing technique called Otsu binarization. Laramy et al. [19] also developed a particle analysis software with customized algorithm and MATLAB image analysis toolbox for detecting the structure of nanoparticles from SEM images. With the recent development in machine vision and deep learning process, researchers have reported automated image processing technique to identify the surface morphology and segment regions of optical or spectroscopy images. Xu et al. [20] identified microstructure properties in SEM images using machine learning (ML) techniques. The developed ML algorithms work efficiently with extreme choreography, distinguishable background, controlled illumination, and high-resolution images. Thus, the background substrate that contains the particles are often chosen to ensure the contrast which help those algorithms to extract a clean particles outline. This is possible when particles are in bulk state, meaning particles are analyzed as raw material before their applications. However, when particles are at the intermediate state of a manufacturing process (work-in-process), the choice for background substrate is limited. In such situation, a heterogeneous particle-substrate (HPS) system will be created rather than just particles. Analyzing particles within a HPS system can be challenging due to lack of contrast high image noises, low image contrasts, uneven illumination and hazy backgrounds as shown in Figure 1.

In response to this challenge, a deep learning object detection algorithm (YOLO) has been put into practical use. Initially, an HPS (heterogeneous particle-substrate) system was created using a wet-deposition particle transfer process that involved the immersion of poly-disperse particles on to a cylindrical substrate. By manipulating the capillary number in the wetdeposition process, four distinct HPS morphologies were captured, each characterized by variations in image heterogeneity. These morphologies were subsequently subjected to detailed analysis. The images were acquired using a VHX 7000 digital 4K microscope (KEYENCE Corporation Ltd., IL) with a magnification of 1000X, covering an area of 300×200 microns. Randomly selected images were designated for both training and testing purposes. The deep learning model is then validated and applied for particle detection and characterization for HPS images with different morphology.



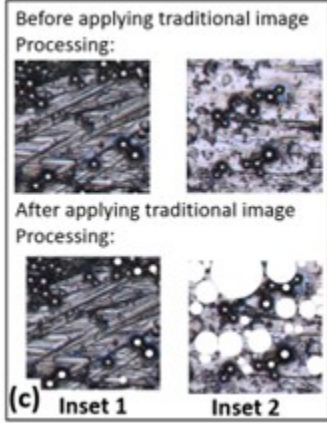


**FIGURE 1**: CONVENTIONAL IMAGE PROCESSING ALGORITHMS APPLIED TO A HETEROGENEOUS IMAGE TAKEN BY VHX 7000 DIGITAL 4K MICROSCOPE AFTER DIP COATING PROCESS. (a) SHOWS THE PARTICLE-SUBSTRATE SYSTEM WITH 80X ZOOM (b) WITH 1000X ZOOM, TWO INSETS SHOW TWO DIFFERENT REGIONS OF THE SAME IMAGE. (c) SHOWS THE EFFECT OF TRADITIONAL IMAGE PROCESSING METHODS APPLIED TO THE TWO INSET IMAGES, WHICH GENERATES COMPLETELY DIFFERENT OUTCOMES FOR SAME INPUT.

### 2. MATERIALS AND METHODS

## 2.1 Heterogeneous Particle-Substrate (HPS) Image Generation

We utilized an in-house wet deposition system to produce heterogeneous Particle-Substrate (HPS) system as shown in Figure 2. Initially, we formulated a polymer solution using Polymethyl Methacrylate (PMMA) and the solvent 1,3 Dioxolane, both sourced from Sigma Aldrich. For this purpose, we utilized nickel-based spherical poly-disperse micro-particles

(Nicrobraz LM; Wall Colomonoy Company, Ohio, Average Diameter 7.56  $\mu$ m) and cylindrical AISI 1006 mild steel (diameter 1.06 mm; ZD Wire Products, Norridgewock, ME) as the substrate material. The metal rod used for the substrate was manufactured through deep drawing, resulting in a surface morphology that is notably rough and irregular. This inherent surface characteristic further contributes to the overall heterogeneity of the captured images.

After stirring for 8 hours, a clear and uniform liquid carrier solution (LCS) is obtained. We then introduced particles into the

LCS to formulate the dipping mixture, ensuring the ratio of the polymer solvent to particles maintains the mixture within the Newtonian regime. We chose cylindrical rods as substrates, and these are dipped through the mixture for particle entrainment, as illustrated in Figure 2. To prevent particle sedimentation during the dipping process, we agitate the mixture to disperse the particles uniformly, forming a 'pseudo-suspension'.

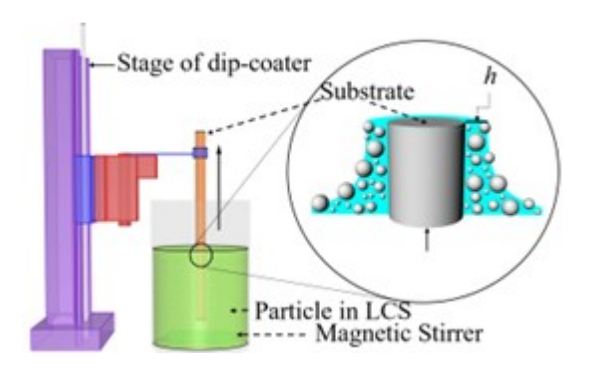


FIGURE 2. SCHEMATIC OF THE WET DEPOSITION SYSTEM.

The rods are dipped into the 'pseudo suspension' at a certain speed at room temperature and atmospheric pressure. A dimensionless capillary number represents the dipping characteristics and resultant particle transfer, which has been discussed in our earlier work [21]. The capillary number of the process depends upon the binder morphology and concentration, particle morphology, solid loading and other dipping parameters. The balance between the viscous drag, and the capillary action during withdrawal facilitate the particle entertainment on the rod substrate. The entrained particles will adhere on the substrate with the dry binder as the solvent evaporates quickly. The particle transfer process is often defined with a dimensionless capillary number. The details of material properties and dipping procedure is discussed in our previous article [22]. The images are taken using VHX 7000 digital 4K microscope (KEYENCE Corporation Ltd., IL) with 1000X magnification (area 300×200 micron) and coaxial full ring lighting.

### 2.2 Application of AI technique

The YOLO (You only look once) is a popular and widely used neural network-based AI algorithm for multiple object detection from an image. It is quick and can successfully detect object from noisy image. Thus, YOLO algorithm is selected in this study for identifying particles. For completeness, we

describe the YOLO algorithm in brief here. Details on YOLO algorithm can be found in the literature [23-26]. YOLO is constructed with single neural network, which can predict the class probabilities and bounding boxes after an image is passed through and resized with grid. These grid cells are responsible for finding the position of the objects. Each grid cell containing the center of the object is accountable for the detection with bounding box. Each predicted bounding box has five parameters: confidence score, coordinate of the center of the bounding box (x,y), and the width and the height of the bounding box (w, h). A bigger bounding box is created with the overlapped bounding boxes which has higher confidence score than the threshold and an Intersection Over Union (IOU) is generated. Other overlapped bounding boxes are removed by Non-Maximum Suppression [23].

Data Set: Five images are selected and cut into 416×416-pixel size creating a total of 258 images are generated. A total 222 images are used as the training set and are annotated and augmented using a web-based annotation software 'roboflow' [27]. 24 images are used for validation and 12 images are utilized for testing purpose. The images are then exported through roboflow to be trainable in YOLOv5 as a custom dataset. We have used google colab for training the model which has two processor cores of 2250 MHz, 12.68 GB of RAM and 1.8 GB of GPU.

### 3. RESULTS AND DISCUSSION

When the substrate is dipped inside the heterogeneous mixture, a thin polymer layer is adsorbed at the solid-liquid interface. The thickness of this thin polymeric layer depends upon the polymer content, type, and dipping speed, which is often defined by a dimensionless capillary number. During the retraction of the substrate, the mixture velocity is directed downward, and the intermolecular forces between mixture and substrate surface help the particles adhere to the substrate. Increased polymer layer thickness facilitates larger particle adhesion while increasing particle volume fraction increase the surface coverage by the particles [21, 22, 28]. As the substrate in our experiment remains the same, the heterogeneity will depend upon the number of adhered particles and their distribution. Based on the various process parameters (e.g., volume fraction of polymer and particles, dipping speed etc.), the heterogeneous particlesubstrate (HPS) image morphology can be classified into four distinct categories: (a) Monodisperse- clustered, Monodisperse- Non-clustered, (c) Polydisperse- clustered and (d) Polydisperse- non-clustered, as shown in Figure 3.

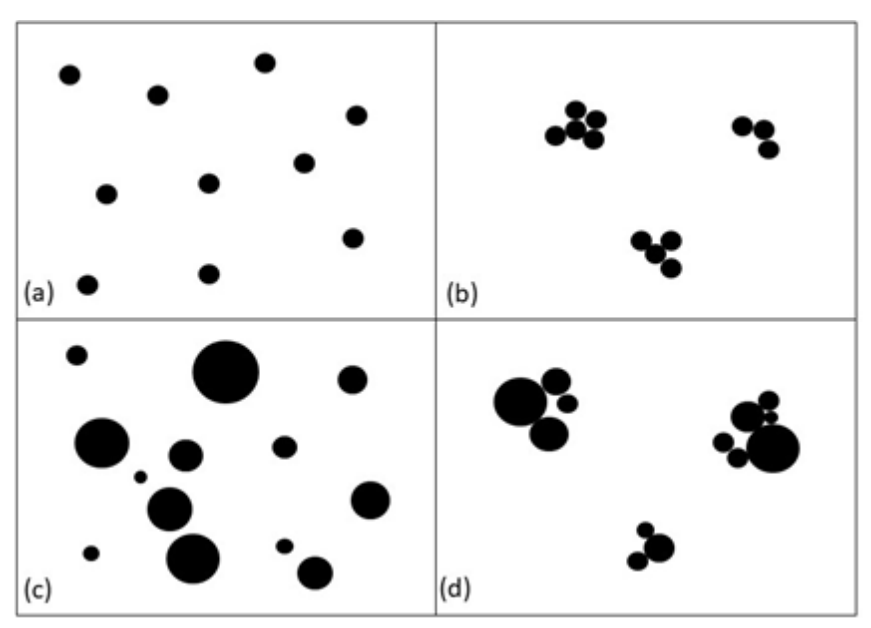


**FIGURE 3**: FOUR TYPES OF PARTICLE DISTRIBUTION: (a) MONODISPERSE NON-CLUSTERED, (b) MONODISPERSE CLUSTERED, (c) POLYDISPERSE NON-CLUSTERED, (d) POLYDISPERSE CLUSTERED.

To compute the performance of our proposed automated particle analysis tool, all four HPS categories are considered for training, testing and validation purpose. The hyper parameters such as model depth multiple and layer channel multiple are used as 0.33 and 0.50 following some trial-and-error experiment. Also, 100 epochs are used to train the model which seems to converge fairly quickly with our datasets. It took less than 6 minutes to train the model and detection of a single image takes about 10 secs. Once the model is trained, tested, and validated with the 258 datasets, the model is used to further implement with completely new sets of images which were never seen before by the algorithm.

During the implementation stage, four categories of images (as discussed in Figure 3) are collected from our experiment discussed earlier. Using the trained model, the particle number is analyzed (over or under-counting) for all four categories and the results are compared with respect to the ground truth shown in Table 1. The ground truth is determined by a domain expert counting individual particle manually. Table 2 shows the total number of actual particles that are present in the respective image counted manually and compared with the total number of

particles counted by our trained tool. In most circumstances, the automated computational tool identified a little-bit more particles (>12%) than the actual count of particles (overcounting). This is because of the heterogeneity on the image discussed earlier and the trained model considers any small dots/noise in the image as a particle. In some instances, the model predicted more particles than actually exist, by taking multiple particles as one and creating a bounding box around them (Figure 4). (Each rectangle is representative of detected bounding box for each particle. In Figure 4(b) and 4(c) a rectangle is generated for two particles combined where each particle already has a bounding box. In Figure 4(d) one particle is covered by a small and a big bounding box.) Additionally, we also cross-checked the number of particles that the model is unable to identify as presented in the Table 1 (under-counting). It can be observed that the trained model is able to detect most particles (accuracy >97%) in such heterogeneous background. This performance off course justifies using automated computational tool based on deep learning approach to analyze particles in a more realistic and in-situ environment.

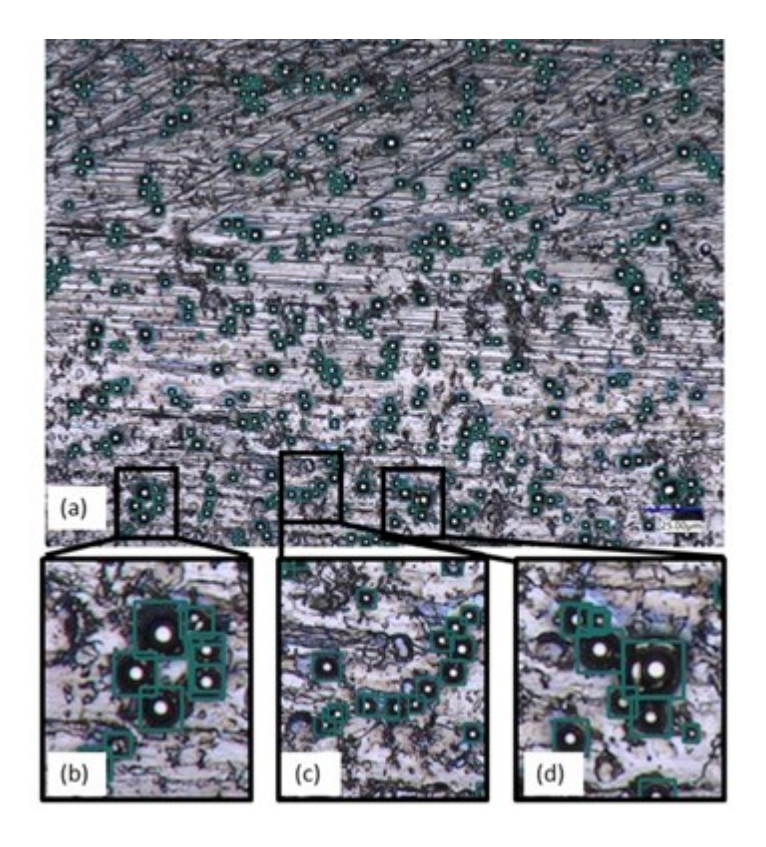


**FIGURE 4**: (a) PARTICLE RECOGNITION BY THE PROPOSED MODEL, INSETS (b), (c), (d) SHOW THE EXAMPLE OF OVERCOUNTING.

Table 1: Comparison between proposed method and ground truth (hand counted) in particle counting operation.

Image Type	Sample Name	Particle count (YOLOv5)	Actual particle count (hand-counted)	Particles could not be identified	Accuracy (%)	Non- particle counted as particle	Percentage of particles overcounted (%)
Monodisperse layer	Sample 1	1663	1597	6	99.62	72	4.85
cluster	Sample 2	553	526	4	99.24	31	
Monodisperse Non-	Sample 3	161	148	1	99.32	14	12.01
Cluster	Sample 4	461	411	3	99.27	53	
Polydisperse layer	Sample 5	216	192	2	98.96	26	11.70
cluster	Sample 6	183	168	1	99.40	16	
Polydisperse layer	Sample 7	130	124	1	99.19	7	9.69
non-cluster	Sample 8	86	76	2	97.37	12	

Particle covering the substrate is often an important measuring matrix, which is also measured and compared using our trained model. The area coverage is calculated using the following equation:

Area coverage = 
$$\sum_{i=1}^{N} \frac{\pi}{4} \left( \frac{w_i + h_i}{2} \right)^2$$
 (1)

Here, w and h are the width and height of the bounding box defined in YOLO respectively. These values are directly obtained by applying the particle recognition model to the images. Since the particle are spherical, the average of the width and height is assumed to be the diameter of the particle. To determine the accuracy of this process, we have taken four smaller pictures cropped from the bigger picture of the size 416×416 pixels and applied the model on them. The evaluated surface coverage from the model is then compared to the ground truth, which is manually measured by a domain expert with the help of a free-form computer-aided-design (CAD) tool, Rhinoceros (Rhino LLC, USA). The non-deformed images are important in the CAD API and the diameter, and the outer perimeter of the particles or particle groups are traced using

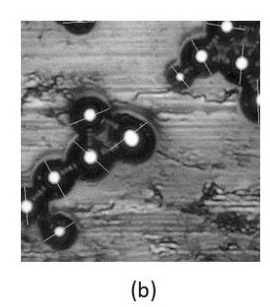
Spline contour. Figure 5(a-c) shows the process of calculating the diameter and outer perimeter of the particles using Rhino as ground truth. Figure 5(d) shows the identified particles with our trained model. The percentage of surface converges found from our trained model and manual method are presented in the Table

2. The manual method is considered as the ground truth and the accuracy is calculated accordingly. We have found a reasonable accuracy of the surface coverage calculation ranges from 80.61% to 95.90%.

Table 2: Comparison of proposed method and ground truth (hand counted) in surface area coverage calculation.

Sample number	Surface Coverage (%) by	Surface Coverage (%) by	Accuracy (%)
	proposed Method	Ground Truth	
1	8.24	9.41	87.61
2	8.76	7.34	80.61
3	20.77	21.65	95.90
4	31.21	26.58	82.59







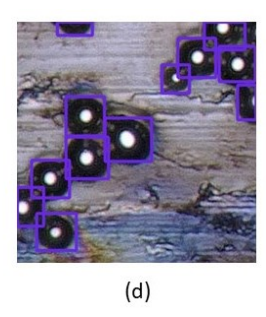


**FIGURE 5**: (a) INPUT IMAGE WITH SIZE 416X416, (b) MANUALLY CALCULATING THE DIAMETER, (c) MANUALLY CALCULATING THE AREA COVERAGE WITH RHINO, (d) PARTICLE DETECTION USING PROPOSED METHOD.

Inaccuracies in surface covering measurement may have occurred due to the assumption that all particles are perfectly circular. However, oblate and prolate particles are not uncommon. For a cluster of particles, the geometry of the enclosing bounding box can slightly change due to the position of the neighboring particles. This changes the shape of the

bounding box from square to rectangular and as a result introduces variation in the surface coverage calculation. The accuracy of the surface coverage can be further improved if the perimeter of the particle can be identified efficiently with other machine learning techniques i.e., semantic segmentation [29, 30] which has not been considered in this paper.

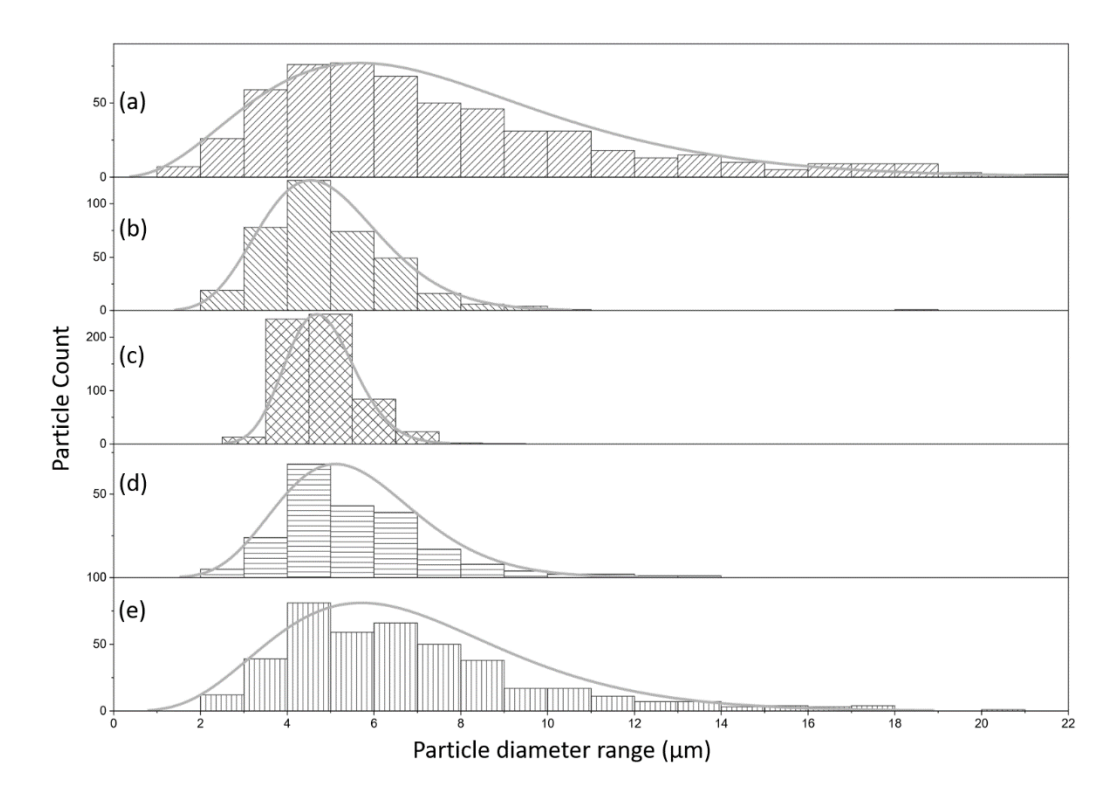


**FIGURE 6**: PARTICLE SIZE DISTRIBUTION OF (a) BULK PARTICLES, AND COMPARED WITH (b) MONODISPERSE-CLUSTERED, (c) MONODISPERSE NON-CLUSTERED, (d) POLYDISPERSE CLUSTERED, (e) POLYDISPERSE NON-CLUSTERED MEASURED WITH THE PROPOSED METHOD.

The image of the bulk particles are captured using SEM after sieving using the Gilson Performer III shaker through Stainless Steel 635 Mesh ( $20\mu m$ ) in our lab. The size distribution of bulk particles is shown in Figure 6(a). The size distribution of coated rod after dip-coating with particle is analyzed using the proposed method as an automatic tool. It can be clearly observed that our algorithm generated distribution matches the anticipated distribution. For example, the size distribution of two monodisperse samples (Figure 6 (b), and 6(c)) have narrower distribution than the poly-disperse samples. The poly-dispersed non-clustered sample (Figure 6 (d)) closely matches the bulk distribution with wider size distribution range as expected.

### 4. CONCLUSION

In this paper we have presented a way of particle size analysis using a deep learning object detection algorithm for heterogeneous particle-substrate (HPS) system. The proposed method detects and counts particles with a very high accuracy even with complex background with different morphology. We can evaluate the quality of sorting by calculating the particle size distribution using the proposed method and find the ideal process parameters for the particle transfer process. The proposed method can be adapted for in-situ measurement of particle size, distribution, and coverage. This in-situ process can be applied to correct the process parameters as this process shows the coated particle distribution immediately after the particle transfer process. Additionally, this algorithm has the potential to reverse

engineer the characteristics of the liquid carrier system, which can be beneficial for industrial applications including diagnosis of blood, wastewater treatment etc.

### **ACKNOWLEDGEMENTS**

Financial supports from Grant NSF-CMMI # 2101745 and US-DOT # 693JK31850009CAAP are acknowledged. The authors also acknowledge the support from UMaine EMPOWER and UMaine-NU Seed Grant for this research.

### **REFERENCES**

- [1] Cordova, L., Campos, M., Tinga, T., Li, H., Ramezani, M., Li, M., Ma, C., & Wang, J. (2017). Powder characterization and optimization for additive manufacturing. Tribol. Int, 128, 926872-926872.
- [2] Samal, P., & Newkirk, J. (2015). Powder metallurgy methods and applications. ASM handbook of powder metallurgy, 7.
- [3] Coan, T., Barroso, G.S., Motz, G., Bolzán, A., & Machado, R.A.F. (2013). Preparation of PMMA/hBN composite coatings for metal surface protection. Materials research, 16(6), 1366-1372.
- [4] Mariello, M., Guido, F., Mastronardi, V.M., Giannuzzi, R., Algieri, L., Qualteri, A., Maffezzoli, A., & De Vittorio, M. (2019). Reliability of protective coatings

- for flexible piezoelectric transducers in aqueous environments. Micromachines, 10(11), 739-739.
- [5] Liu, W., Li, J., Huang, X., & Bi, J. (2021). Corrosion protection of Q235 steel using epoxy coatings loaded with calcium carbonate microparticles modified by sodium lignosulfonate in simulated concrete pore solutions. Materials, 14(8), 1982-1982.
- [6] Holtzer, M., & Kmita, A. (2020). Mold and Core Sands in Metalcasting: Chemistry and Ecology. Sustainable Development.
- [7] Baumeister, P. (2004). Optical coating technology (Vol. 137). SPIE press.
- [8] Stewart, J.W., Akselrod, G.M., Smith, D.R., & Mikkelsen, M.H. (2017). Toward multispectral imaging with colloidal metasurface pixels. Advanced Materials, 29(6), 1602971-1602971.
- [9] Köstlin, H., Frank, G., Hebbinghaus, G., Auding, H., & Denissen, K. (1997). Optical filters on linear halogen-lamps prepared by dip-coating. Journal of non-crystalline solids, 218, 347-353.
- [10] Abubakar, A.A., Yilbas, B.S., Al-Qahtani, H., Alzaydi, A., & Alhelou, S. (2020). Environmental dust repelling from hydrophobic and hydrophilic surfaces under vibrational excitation. Scientific reports, 10(1), 1-19.
- [11] Khoda, B., Ahsan, A.M.M.N., & Shovon, S.M.N. (2021). Dip Coating From Density Mismatching Mixture. Journal of Micro and Nano-Manufacturing, 9(2).
- [12] Underwood, S.J., Gorham, J.M., & others. (2017). Challenges and approaches for particle size analysis on micrographs of nanoparticles loaded onto textile surfaces. NIST Special Publication, 1200, 22-22.
- [13] Kumara, G.H.A.J.J., Hayano, K., & Ogiwara, K. (2012). Image analysis techniques on evaluation of particle size distribution of gravel. GEOMATE Journal, 3(5), 290-297.
- [14] Berardi, A., Bisharat, L., Blaibleh, A., Pavoni, L., & Cespi, M. (2018). A simple and inexpensive image analysis technique to study the effect of disintegrants concentration and diluents type on disintegration. Journal of Pharmaceutical Sciences, 107(10), 2643-2652.
- [15] Lee, M.-J., Seo, D.-Y., Lee, H.-E., Wang, I.-C., Kim, W.-S., Jeong, M.-Y., & Choi, G.J. (2011). In line NIR quantification of film thickness on pharmaceutical pellets during a fluid bed coating process. International journal of pharmaceutics, 403(1-2), 66-72.
- [16] He, H., Wang, Y., Farkas, B., Nagy, Z.K., & Molnar, K. (2020). Analysis and prediction of the diameter and orientation of AC electrospun nanofibers by

- response surface methodology. Materials & Design, 194, 108902-108902.
- [17] Mondini, S., Ferretti, A.M., Puglisi, A., & Ponti, A. (2012).**PEBBLES** and PEBBLEJUGGLER: software for accurate. unbiased. and measurement and analysis of nanoparticle morphology from transmission electron microscopy (TEM) micrographs. Nanoscale, 4(17), 5356-5372.
- [18] Phromsuwan, U., Sirisathitkul, C., Sirisathitkul, Y., Uyyanonvara, B., & Muneesawang, P. (2013). Application of image processing to determine size distribution of magnetic nanoparticles. Journal of Magnetics, 18(3), 311-316.
- [19] Laramy, C.R., Brown, K.A., O'Brien, M.N., & Mirkin, C.A. (2015). High-throughput, algorithmic determination of nanoparticle structure from electron microscopy images. ACS nano, 9(12), 12488-12495.
- [20] Xu, H., Liu, R., Choudhary, A., & Chen, W. (2015). A machine learning-based design representation method for designing heterogeneous microstructures. Journal of Mechanical Design, 137(5), 51403-51403.
- [21] Shovon, S.M., Alam, A., Gramlich, W., & Khoda, B. (2022). Micro-particle entrainment from density mismatched liquid carrier system. Scientific Reports, 12(1), 1-13.
- [22] Khalil, I., & Khoda, B. (2022). Sorting of Poly-Disperse Particle by Entrapment Using Liquid Carrier System. Journal of Manufacturing Science and Engineering, 144(5).
- [23] Redmon, J., Divvala, S., Girshick, R., & Farhadi, A. (2016). You only look once: Unified, real-time object detection. In Proceedings of the IEEE conference on computer vision and pattern recognition.
- [24] Redmon, J., & Farhadi, A. (2017). YOLO9000: better, faster, stronger. In Proceedings of the IEEE conference on computer vision and pattern recognition.
- [25] Redmon, J., & Farhadi, A. (2018). Yolov3: An incremental improvement. arXiv preprint arXiv:1804.02767.
- [26] Bochkovskiy, A., Wang, C.-Y., & Liao, H.-Y.M. (2020). Yolov4: Optimal speed and accuracy of object detection. arXiv preprint arXiv:2004.10934.
- [27] Roboflow.
- [28] Khoda, B., Nazmul Ahsan, A.M.M., & Shovon, S.M.N. (2021). Solid Transfer of Large Particles by Dipping in a Heterogeneous Mixture. In International Manufacturing Science and Engineering Conference.
- [29] Long, J., Shelhamer, E., & Darrell, T. (2015). Fully convolutional networks for semantic segmentation. In

- Proceedings of the IEEE conference on computer
- vision and pattern recognition.
  [30] Garcia-Garcia, A., Orts-Escolano, S., Oprea, S., Villena-Martinez, V., & Garcia-Rodriguez, J. (2017). A review on deep learning techniques applied to semantic segmentation. arXiv preprint arXiv:1704.06857.